Title
Antiferromagnetic domain switching modulated by an ultrathin Co interlayer in the Fe/Co/CoO/MgO(001) system

Journal
Physical Review B, 102(2)

ISSN
2469-9950

Authors
Yang, Yu
Liang, Jianhui
Li, Qian
et al.

Publication Date
2020-07-01

DOI
10.1103/physrevb.102.024434

Peer reviewed

Antiferromagnetic domain switching modulated by an ultrathin Co interlayer in the Fe/Co/CoO/MgO(001) system

Yu Yang,[1] Jianhui Liang,[1,*] Qian Li,[2] Gong Chen,[3] Chao Zhou,[1] Jia Xu,[1] Lu Sun,[1] Mengmeng Yang,[2] Alpha T. N'Diaye,[4] Zi Qiang Qiu,[2] and Yizheng Wu[1,5,*]

[1]*Department of Physics, State Key Laboratory of Surface Physics, Fudan University, Shanghai 200433, People's Republic of China*

[2]*Department of Physics, University of California at Berkeley, Berkeley, California 94720, USA*

[3]*NCEM, Molecular Foundry, Lawrence Berkeley National Laboratory, Berkeley, California 94720, USA*

[4]*Advanced Light Source, Lawrence Berkeley National Laboratory, Berkeley, California 94720, USA*

[5]*Shanghai Research Center for Quantum Sciences, Shanghai, 201315, China*

Using a combination of hysteresis loop, Kerr microscope, and x-ray magnetic circular dichroism measurements, we investigated the antiferromagnetic (AFM) domain switching process modulated by the sub-nm thick Co inserting layer in a single crystalline Fe/Co/CoO/MgO(001). The CoO AFM domain switching occurs at lower temperature for the thicker Co interlayer, and the activation energy barrier of CoO AFM domain switching decreases as the Co interlayer thickness increases. The exchange coupling strength between the AFM spins in CoO layer and the ferromagnetic spins in the Fe/Co bilayer is found to be independent of the Co layer thickness. Our results suggest an approach to modulate the dynamic properties of AFM domains with an interfacial modification.

I. INTRODUCTION

The dynamics of magnetization reversal is crucial to understanding fundamental magnetism and developing high performance spintronics devices [1–5]. Most studies in the field are focused on ferromagnetic (FM) materials, based on which numerous numbers of spintronics devices were rapidly developed. In contrast, magnetization reversal in antiferromagnetic (AFM) materials has been much less explored due to its zero net magnetic moment. Recently, there arises an increasing interest in employing AFM materials in the generation, transport, and detection of spin current for future spintronic devices [6–11]. The demonstration of current-induced switching of AFM domains [12–17] enables the functionality of storing information with the variable domain status in AFM spintronics devices [18]. Therefore, the AFM domain switching process has become one of the critical issues in further developing the spintronics technology based on AFM materials.

In FM/AFM systems, the FM magnetization switching is highly correlated with AFM magnetization switching due to the interface exchange coupling. AFM domain evolution has been previously investigated to a certain extent in the studies on the time-dependent exchange bias effect (usually referred to as the training effect) [19–22]. However, most studies on training effect were performed in polycrystalline systems, thus random spin orientations of AFM polycrystalline grains prohibit the explicit understanding of the AFM spin switching process. The single-crystalline system has been applied to study the physics during the AFM spin switching process. For instance, utilizing the x-ray magnetic linear dichroism measurements, the CoO AFM spins were found to be perpendicularly coupled with the Fe FM spins in single-crystalline Fe/CoO(001) bilayers [23,24] due to spin-flop coupling [25,26]. Rotatable AFM CoO spins were identified in response to the Fe magnetization reversal [27]. The 90°-switching process of CoO AFM domain driven by the exchange coupling was revealed by measuring the Fe remanent Kerr signal, and the AFM domain switching energy barrier can be characterized through a temperature-dependent measurement [28]. The AFM domain switching energy barrier in the Fe/CoO(001) system decreases with the applied field due to the spiral-like spin configuration in the Fe layer, which can be tailored by the field strength [29]. Generally speaking, the AFM domain evolution in a FM/AFM system is driven by the exchange coupling between FM and AFM layers, thus the magnetic property at the AFM/FM interface plays important role on AFM domain switching in the Fe/CoO(001) system. However, the interface effect on the AFM domain switching still remains uninvestigated.

In this paper, we report the modulation effect on the AFM domain switching process by inserting the sub-nm Co layers at the Fe/CoO interface in the Fe/CoO/MgO(001) system. The excitation energy barrier for CoO AFM domain switching was determined to strongly decrease with the thickness of inserted Co layer. However, both magnetic loop measurements and x-ray magnetic circular dichroism (XMCD) measurements indicate that the FM/AFM interface exchange coupling remains unchanged with the inserted Co layer. Our results suggest that AFM domain switching can be influenced by the interfacial modification.

*Corresponding authors: jianhuiliang13@fudan.edu.cn; wuyizheng@fudan.edu.cn

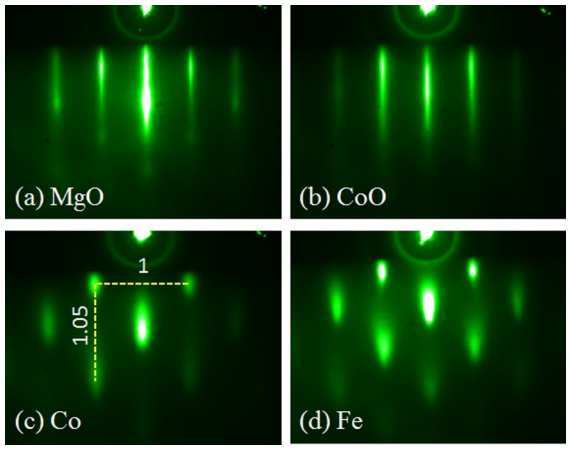

FIG. 1. Typical RHEED patterns of (a) MgO(001), (b) CoO (4.5 nm)/MgO(001), (c) Co(0.7 nm)/CoO(4.5 nm)/MgO(001), and (d) Fe(34 nm)/Co(0.7 nm)/CoO(4.5 nm)/MgO(001) with the electron incident direction along MgO⟨110⟩.

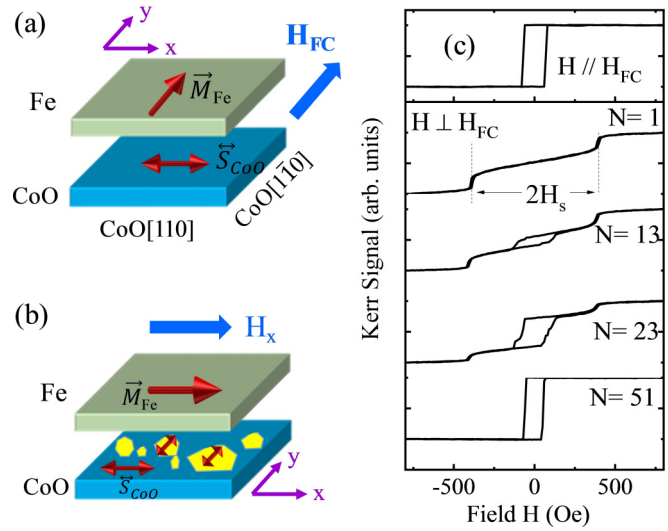

FIG. 2. (a) Schematics of spin configurations in the Fe/CoO bilayer after field cooling. (b) Schematics of CoO AFM domain switching after the field sweeping cycles with the applied field perpendicular to the field cooling direction. (c) Hysteresis loops from Fe (34 nm)/CoO (4.5 nm)/MgO(001) at 107 K for $H \parallel H_{FC}$ and $H \perp H_{FC}$ during the magnetic field cycling. N denotes the cycling number.

II. EXPERIMENTS

Fe/Co/CoO/MgO(001) films were prepared by molecular beam epitaxy in an ultrahigh vacuum chamber with a base pressure of 2×10^{-10} Torr. The single-crystal MgO(001) substrates were first cleaned with acetone, followed by annealing at 600 °C for 30 min in ultrahigh vacuum. A 10-nm MgO seed layer was deposited at 500 °C by e-beam evaporation before the Fe/Co/CoO growth. The CoO film was grown by reactive deposition of Co at an oxygen pressure of 5.0×10^{-7} Torr at room temperature [30,31]. Subsequently, the Fe/Co bilayer was grown on top of the CoO layer at room temperature. The Co layer was grown into a step or wedge shape by moving the substrate behind a knife-edge shutter along the MgO⟨110⟩ direction. All the Film thicknesses were determined by the growth rate measured by a calibrated quartz thickness monitor. In this study, the growth rate was ∼0.2 nm/min for Co, and ∼0.7 nm/min for Fe. The reflection high energy electron diffraction (RHEED) patterns in Fig. 1 reveal good epitaxy growth of the CoO, Co, and Fe films. Note that the separation ratio between the diffraction spots in the RHEED pattern from the Co film in Fig. 1(c) is 1.05, different from the ratio of $\sqrt{2}$ for the face-centered-cubic structure, but close to the ratio of 1 for the body-centered-cubic structure, thus the thin Co film on CoO(001) surface likely has the metastable body-centered-tetragonal structure. All the films have the lattice relation of Fe[100]//Co[100]//CoO[110]//MgO[110] with the (001) crystalline orientation. Finally, the samples were covered with a MgO layer as the protecting layer, where the thickness of MgO layer is 4 nm for magneto-optic Kerr effect (MOKE) measurements and 2 nm for XMCD measurements.

The magnetic properties of the Co step-shaped films were measured by the longitudinal MOKE using a laser diode with a wavelength of 670 nm. In the MOKE measurement, the light incident angle is 45°, and the magnetic field was applied in the film plane by a vector magnet, which allows the variable in-plane field cooling directions, e.g., perpendicular or parallel to the field scanning direction. The sample temperature is varied between 80 and 330 K in an optical Dewar cooled by liquid nitrogen. The in-plane magnetic domain images were taken by a commercial Evico Kerr microscopy [32]. The XMCD measurements on the Fe/Co/CoO/MgO(001) sample with the Co wedge was performed with the total electron yield mode at the beamline 6.3.1 at the Advanced Light Source.

III. RESULTS AND DISCUSSION

In a Fe/CoO(001) system, the AFM CoO domain switching energy barrier is related to the interfacial exchange coupling, therefore it is sensitive to the interface properties. In order to study how the interface property influences the AFM domain switching, we prepared a sample of Fe(34 nm)/Co(d_{Co})/CoO(4.5 nm) with the thickness of Co interlayer d_{Co} ranged from 0 to 1 nm. The Co interlayer was grown into a step shape with different thickness. The width of each step is 1 mm, smaller than the size of the laser beam in MOKE measurement. The film preparation condition is same for all the samples except the Co thickness, thus we can systematically study how the interface Co layer influence the CoO AFM domain switching.

In the single crystalline Fe/CoO/MgO(001) system, the CoO AFM spin has the in-plane fourfold anisotropy with the easy axis (EA) along the CoO⟨110⟩ direction [30,31]. After field cooling along the CoO⟨110⟩ direction, the interfacial spin-flop coupling aligns the CoO AFM spins S_{CoO} perpendicularly to the cooling field H_{FC} [Fig. 2(a)], and subsequently induces an in-plane uniaxial magnetic anisotropy in the Fe film with the EA parallel to H_{FC}. The magnetic hysteresis loop exhibits an EA square loop when $H \parallel H_{FC}$, and the double-split hard-axis (HA) when $H \perp H_{FC}$, as shown in Fig. 2(c) [28,29]. The magnitude of this exchange-coupling induced uniaxial anisotropy can be retrieved from the splitting field H_S of the HA double-split loop, shown in Fig. 2(c). The

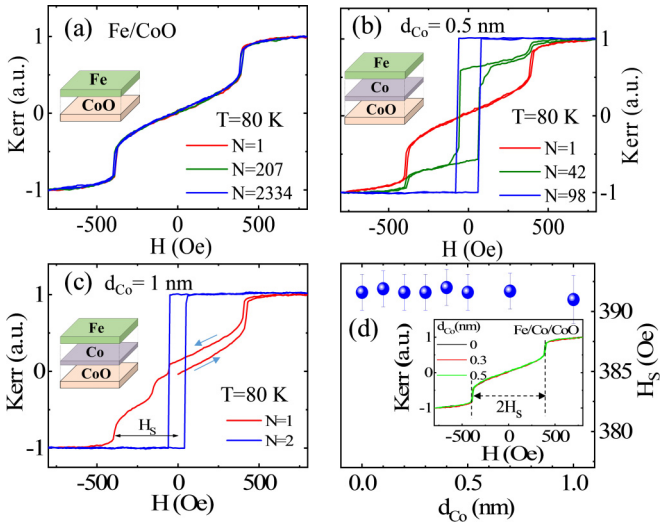

FIG. 3. Representative hysteresis loops of (a) Fe(34 nm)/CoO(4.5 nm), (b) Fe(34 nm)/Co(0.5 nm)/CoO(4.5 nm), and (c) Fe(34 nm)/Co(1 nm)/CoO(4.5 nm) for $H \perp H_{FC}$ at 80 K during magnetic field cycling (N denotes the cycling number). The loop with $N = 1$ in (c) starts from the initial state right after field cooling process. (d) Co thickness dependence of splitting field H_S in the Fe/Co/CoO system. The inset indicates the identical hysteresis loops with different Co interlayer thickness.

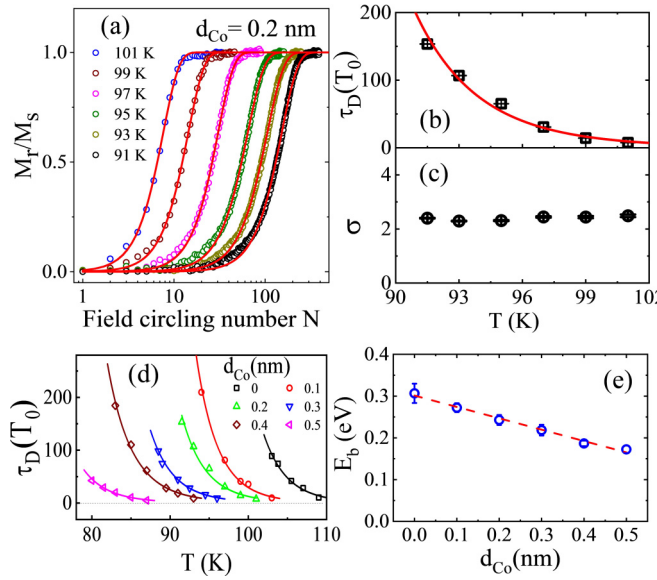

FIG. 4. (a) Remanent Kerr signal versus field cycling number N at different temperatures from the sample of Fe (34 nm)/Co(0.2 nm)/CoO (4.5 nm)/MgO(001). The red lines are the fitted results using Eq. (1). (b) and (c) Temperature dependence of the fitted τ_D and σ, respectively. The red line in (b) is the fitting curve with Eq. (2). (d) Temperature-dependent relaxation time constant τ_D for Fe/Co/CoO/MgO(001) with various Co thicknesses. The solid lines are fitted results with Eq. (2). (e) The energy barrier from the fitting as a function of the Co thickness. The dashed line is the linear fitting.

exchange bias in Fe/CoO/MgO(001) is negligible in comparison with the much stronger uniaxial anisotropy because of the compensated spin configuration on CoO(001) surface. However, CoO AFM spins S_{CoO} can be switched by 90° from $S_{CoO} \parallel H$ to $S_{CoO} \perp H$ by continuously sweeping the field H perpendicular to H_{FC} due to strong interfacial exchange coupling and thermal activation, thus the CoO AFM domains with the spins perpendicular to the applied field will appear and propagate driven by the interfacial exchange coupling [Fig. 2(b)]. Then, the HA loop gradually changes to the EA square loop at a certain temperature, as shown in Fig. 2(c). Due to strong exchange coupling at the Fe/CoO interface, the Fe FM domain is strongly coupled with the underneath CoO AFM domain, therefore the remanence Kerr signal from Fe film represents the fractional area of the switched CoO spins [28].

It is already known that the AFM switching induced by the thermal activation strongly depends on the temperature, i.e., the switching probability of CoO AFM spins strongly decreases at lower temperature. Figure 3(a) shows the HA loops with $H \perp H_{FC}$ of Fe/CoO bilayer measured at 80 K, and the identical loops are found after thousands of field cycles, which suggests that CoO AFM spins are robust at 80 K and cannot be switched by the Fe FM spins reversal. However, we found that the AFM domain switching probability increases significantly with the Co interlayer thickness. Figure 3(b) shows that the hysteresis loop in Fe/Co(0.5 nm)/CoO gradually evolves from a HA loop into an EA loop after dozens of times field sweeping. In the Fe/Co(1 nm)/CoO sample, the loop becomes an EA shape after the half circle of the field sweeping [Fig. 1(c)]. Considering the field sweeping induced transition of hysteresis loops originates from the AFM domain switching, the results in Fig. 3 indicates that the insertion of Co layer between Fe and CoO significantly lowers down the energy barrier of AFM domain switching.

We found that the decrease of the AFM domain switching barrier may not be related to the change of the interfacial exchange coupling. The splitting field H_S of the double-split loops is proportional to K_u/M, where K_u is the uniaxial anisotropy induced by the interfacial exchange coupling, and M is the total magnetization of the system. As shown in Fig. 3(d), H_S is independent of the Co thickness. Our sample contains 34 nm Fe, thus M only changes very little with the additional sub-nm Co layer at the interface. Although the Kerr signal only comes from the top ~20 nm Fe film, the measured hysteresis loop should change accordingly by the change of interfacial exchange coupling. Therefore, we conclude that the uniaxial anisotropy induced by the interfacial exchange coupling does not change with the Co layer thickness.

To get a better understanding on the mechanism of AFM switching process, we investigated the temperature dependence of CoO AFM spin switching in the Fe/Co/CoO systems with different Co thicknesses. As shown in Figs. 2 and 3, during the cycles of field sweeping, the remanence signal from the Fe film gradually changes from 0 to 1. Due to the strong interfacial exchange coupling, the Fe magnetization is expected to be always perpendicular to the CoO AFM spins at the remanent state, thus the ratio between the remanence Kerr signal (M_r) and the saturation signal (M_S) along the Fe hard axis is proportional to the fractional area of switched CoO AFM domains. Figure 4(a) shows the remanence signal as a function of the field cycling number at different temperatures

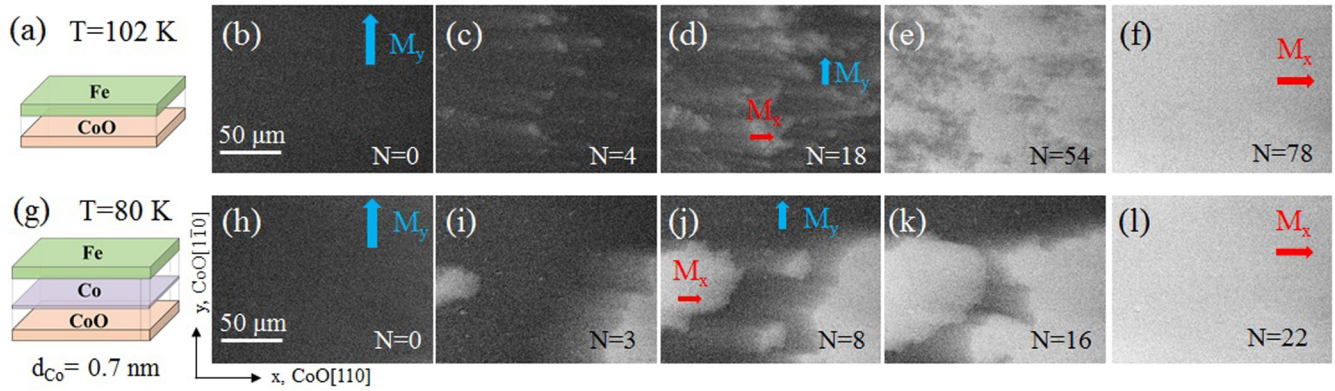

FIG. 5. (a) Schematic drawing of sample structure of Fe (34 nm)/CoO (4.5 nm). (b)–(f) Time-dependent domain evolution of Fe/CoO at remanent state after different numbers of field cyclings at 102 K with H decreased from a positive field (+800 Oe). The field cycling number N during the Kerr domain imaging is listed in each frame. (g) Schematic drawing of sample structure of Fe (34 nm)/Co(0.7nm)/CoO (4.5 nm). (h)–(l) Time-dependent remanent domain evolution of Fe/Co/CoO at 80 K.

at $d_{\mathrm{Co}} = 0.2$nm. During the measurement, the field is swept up to 800 Oe, far above the splitting field H_S shown in Fig. 3. With increasing temperature, the cycling time N for AFM domain switching dramatically decreases. The switching of the CoO AFM domain is a combination process of domain nucleation and growth, which can be described by the Kolmogorov-Avrami (KA) model [5,33,34]. The CoO AFM domain switching process can be described by the extended exponential formula:

$$M_{\mathrm{r}}(N)/M_{\mathrm{s}} = 1 - \exp(-(\mathrm{N}/\tau_D)^{\sigma}), \qquad (1)$$

where N is the number of field cycling, σ is a power index, and τ_D is the relaxation time constant charactering the typical time for CoO AFM domain switching with the unit of the time cost T_0 in each loop scan. In our measurement, T_0 usually is $\sim$15 s . The Kerr remanence data in Fig. 4(a) can be well fitted by Eq. (1), indicating that the KA model is valid to describe the AFM CoO switching process.

Figures 4(b) and 4(c) show the fitted τ_D and σ as a function of temperature from Fig. 4(a). While the fitted value of σ shows a constant value around 2.4, the τ_D value decreases exponentially with the Arrhenius law:

$$\tau_D = \tau_0 \exp(E_b/k_{\mathrm{B}}T). \qquad (2)$$

Here τ_0 is a characteristic attempt time with the time unit of T_0, E_b is the energy barrier of the CoO AFM domain, T is the sample temperature, and k_{B} is the Boltzmann constant. By fitting the results of Fig. 4(b) with Eq. (2), we obtain the energy barrier of $E_b = 0.24 \pm 0.01$ eV for the system with a 0.2 nm Co inserting layer.

We further studied the temperature-dependent τ_D on the samples with different d_{Co}, and calculated the energy barrier of AFM switching by fitting τ_D in Fig. 4(d) using Eq. (2). The CoO AFM domain can be switched quickly even at 80 K for the Co layer thicker than 0.6 nm, allowing the quantitative analysis of the temperature-dependent measurements for $d_{\mathrm{Co}} < 0.6$ nm. The fitted energy barriers in Fig. 4(e) show that the AFM switching energy barrier decreases with the interlayer Co thickness in an approximate linear relation. Based on the simple linear extrapolation, the energy barrier for the system with a 1 nm Co interlayer is only 0.03 eV, which is comparable with the thermal energy. This is also consistent with the fast switching of the AFM domains with 1 nm Co interlayer at 80 K, shown in Fig. 3(c).

To observe the effect of the inserted Co layer on AFM domain switching, we performed magnetic domain imaging measurements on Fe (34 nm)/CoO (4.5 nm) bilayer and on Fe (34 nm)/Co(0.7 nm)/CoO (4.5 nm) sandwich using a Kerr microscope. The samples were first cooled down with $H_{\mathrm{FC}} \parallel y$ to align the CoO spins to $S_{\mathrm{CoO}} \parallel x$, where the x axis and y axis correspond to the CoO[110] and [$\bar{1}$10] axes, respectively. Then, the remanent FM domain images of Fe layer were taken after applying a positive field $+H$ and a negative field $-H$ at different cycling times N along the Fe hard axis ($H \parallel x$) [28]. During the field cycling, the maximum strength of the applied field H is 800 Oe, which ensures the saturation of Fe moments (Fig. 3). Right after field cooling, the remanent domain is a single domain with the Fe magnetization $M_{\mathrm{Fe}} \parallel y$, which indicates that $S_{\mathrm{CoO}} \parallel x$. After a few cycles, magnetic domains with $M_{\mathrm{Fe}} \parallel x$ appear, which means the AFM domain with $S_{\mathrm{CoO}} \parallel y$ has formed. While increasing the field cycles, domains with $M_{\mathrm{Fe}} \parallel x$ keep appearing and expanding, eventually forming a single domain with $M_{\mathrm{Fe}} \parallel x$. In this situation, the AFM spin S_{CoO} has completely switched from the x direction to the y direction. To capture the domain evolution at the similar time scale in Fe/CoO and Fe/Co/CoO systems with different domain switching energy barriers, the experimental temperature is 102 K for the Fe/CoO sample, and 80 K for the Fe/Co/CoO sandwich. In Fe/CoO bilayer [Figs. 5(b)–5(f)], the domain evolution process shows the multiple small domains. However, for Fe/Co/CoO sandwich [Fig. 5(h)-5(l)], there are only very few domains nucleated, which eventually expand into the whole area. Such different behavior indicates that the AFM domain in the Fe/Co/CoO system is much easier to expand, implying that the inserted Co layer significantly reduces the energy barrier of the domain wall motion in AFM switching process.

To check how the magnetic property at Fe/CoO interface altered in the presence of the Co layer, we performed the XMCD measurements in the Fe/Co/CoO system as a function of Co thickness. The sample MgO(2 nm)/Fe(2 nm)/Co(wedge) /CoO(4.5 nm) was prepared on MgO(001)

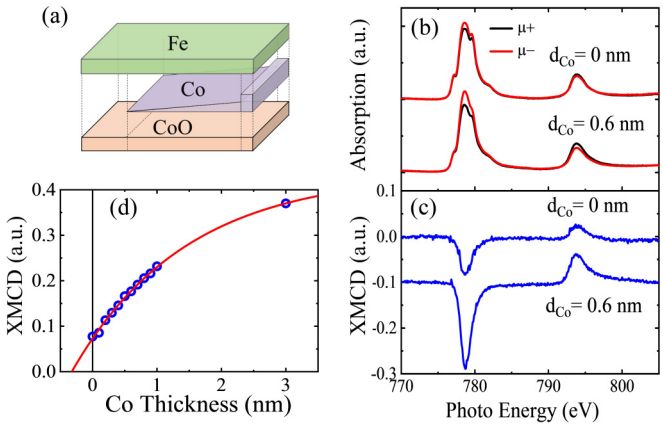

FIG. 6. (a) Schematic drawing of sample structure. (b) Co $L_{2,3}$ x-ray adsorption spectra and (c) XMCD spectra of Fe (2 nm)/CoO (4.5 nm) and Fe (2 nm)/Co(0.6 nm)/CoO (4.5 nm). (d) Co thickness dependent XMCD measured on the Fe(2 nm)/Co (wedge)/CoO (4.5 nm) sample. The solid line is the fitting curve.

substrate, and the thickness of Co wedge continuously changes from 0 to 1 nm with a 3-nm-thick shoulder, which is illustrated in Fig. 6(a). The 2-nm Fe is thin enough for probing the signal from the underneath Co layer with the XMCD measurement. It is reasonable to assume the same Co interlayer properties in Fe/Co/CoO/MgO(001) systems with $d_{\mathrm{Fe}} = 2\,\mathrm{nm}$ and $d_{\mathrm{Fe}} = 34\,\mathrm{nm}$. Figures 6(b) and 6(c) show the typical x-ray absorption and XMCD spectra of Fe/CoO and Fe/Co/CoO. The Co XMCD spectrum from the Fe/CoO system is different from the XMCD spectrum of Co^{2+} [35], but similar to that as the metallic Co film [36]. So, our results indicate that the Fe film metalize the interfacial Co ions at Fe/CoO interface and induce the interfacial Co FM spins [24]. The XMCD signal is stronger with the Co inserting layer in the Fe/Co/CoO films. Figure 6(d) shows the XMCD signal at the Co L_3 edge as a function of Co thickness, which can be well fitted with $A_0(1 - \exp(-(d_{\mathrm{Co}} - d_0)/\lambda))$. Here, A_0 is the saturation XMCD signal, λ is a phenomenological parameter that results from the secondary electron escape depth and the x-ray penetration depth [37], and d_0 is the thickness of the Co layer at Fe/CoO interface metalized by the FM layer. The fitted λ is 1.8 ± 0.1 nm, close to the value obtained from the single layer Co films [37]. The fitted value of d_0 is 0.32 ± 0.02 nm, indicating that, even in the Fe/CoO bilayer, there is a 0.32 nm FM Co metalized layer between the Fe layer and the CoO layer. The good fitting in Fig. 6(d) suggests that the Co interface layer in the Fe/CoO interface has the same magnetic properties as the top Co layer grown intensively, so the interfacial exchange coupling in Fe/Co/CoO systems does not change by the Co inserting layer.

So far, the dynamical switching process of AFM domain has been rarely investigated in literatures, and the mechanism of the CoO AFM domain switching modulated by the Co inserting layer is not clear. However, it is reasonable to compare with its counterpart of the mechanism of FM domain switching under the reversal field. It is well known that, under the driving force of Zeeman energy due to the magnetic field, the FM domain switching happens with the domain nucleation and the domain wall propagation, and the wall pinning or depinning process is important for the domain wall propagation. In our study, the driving force of CoO AFM domain switching is the exchange coupling between FM Fe spins and AFM CoO spins. Since Fig. 3(d) demonstrates that the hysteresis loops are almost unchanged by the Co inserting layer, it is very likely that the interfacial exchange coupling has no change with the Co interlayer thickness. Figure 5 indicates that the domain wall propagation process is significantly changed by the Co layer, thus we suspect that the wall pinning and depinning process are significantly influenced by the Co interlayer layer. Usually the wall pining is associated with the magnetic defects, and it is reasonable that the interfacial magnetic defects of the AFM CoO layer can be modified by the additional Co layer. Based on the X-ray absorption spectrum (XAS) measurements, Abrudan *et al.* showed the evidence of Fe oxidation in the Fe/CoO/Ag(001) system with the Fe film thickness of ∼0.07 nm, but such a weak XAS signal from Fe oxidation is hard to be identified for the Fe thickness above 0.3 nm [24]. The presences of metalized Co and oxidized Fe certainly prove the existence of magnetic defects in the AFM CoO layer near the Fe/CoO interface, and the interface CoO does not remain stoichiometric. Ali *et al.* [38] has shown that the irreversible thermoremanent magnetization in the magnetically diluted AFM $Co_{1-y}O(001)$ layer is responsible for the training effect of the exchange bias in $Co/Co_{1-y}O(001)$ bilayer, so the magnetic defects at the Fe/CoO interface can greatly influence the magnetic dynamics process. The magnetic defects in the AFM CoO layer in the Fe/Co/CoO(001) system can change with the Co layer thickness, since the formation of interfacial Fe oxide is certainly suppressed by the Co inserting layer.

Recently, we reported that the activation energy barrier of CoO AFM domain switching in the Fe/CoO(001) system strongly decreases with the applied magnetic field, and this behavior was attributed to the FM noncollinear spin profile during its magnetization reversal [29]. It is possible that the FM spin structure near the CoO interface is modulated by the Co layer due to the difference of the anisotropy and exchange coupling constant between Fe and Co layers. In this case, the presence of the modulated FM spin profile at the FM/AFM could induce a very different reversal process, contradicting the nearly identical hysteresis loops with different Co thickness shown in Fig. 3. Therefore, the reduced AFM domain switching energy barrier is unlikely attributed to the change of the FM spin profile at FM/AFM interface with different Co layer thickness.

On the other hand, in our measurements on the FM/AFM system, the CoO AFM domain switching can only be quantified indirectly by the remanence Kerr signal from the FM layer. During periodical circling of +H and −H in our measurements, the FM magnetization will be rotated accordingly, which will drive the rotation of AFM spins. So far, the effect of the FM magnetization reversal on the AFM domain switching is still unclear, which may be identified by imaging the AFM domains under the fixed magnetic field. Recently, we reported that the AFM NiO domain can be imaged via the magneto-optical birefringence effect using an optical microscope [39], which may provide an appropriate method to

investigate the dynamic properties of the AFM domains under strong static magnetic field.

IV. SUMMARY

In summary, we investigated the AFM domain switching in epitaxially grown Fe/Co/CoO/MgO(001) modulated by an ultrathin Co inserting layer. Both MOKE hysteresis loops and Kerr microscopy results demonstrate that the energy barrier decreases with the Co inserting layer thickness, and the domain wall motion of the nucleated AFM domain is dominant in the CoO AFM spin switching process for thicker Co inserting layer. Based on the hysteresis loop measurement and the XMCD measurement, the interfacial exchange coupling strength between FM and AFM spins is found to be unchanged by the Co inserting layer. To understand the modulation of AFM domain switching energy by the Co inserting layer, it requires a deeper understanding of the physical mechanism of the AFM domain nucleation and AFM domain wall depinning and propagation. Our studies not only present a different way to control the AFM domain switching by the interface modulation, but also call for future investigation on the AFM domain switching mechanism, which is essential for AFM spintronics study.

ACKNOWLEDGMENTS

This work was supported by the National Key Research and Development Program of China (Grant No. 2016YFA0300703), National Natural Science Foundation of China (Grants No. 11974079 and No. 11734006), and by Shanghai Municipal Science and Technology Major Project (Grant No. 2019SHZDZX01). The work at the Molecular Foundry and the Advanced Light Source, Lawrence Berkeley National Laboratory, was supported by the Office of Science, Office of Basic Energy Sciences, Scientific User Facilities Division, of the U.S. Department of Energy under Contract No. DE-AC02-05CH11231. The work at Department of Physics, University of California at Berkeley was supported by U.S. Department of Energy, Office of Science, Office of Basic Energy Sciences, Materials Sciences and Engineering Division under Contract No. DE-AC02-05CH11231 (van der Waals heterostructures program, KCWF16).

[1] M. Yamanouchi, J. Ieda, F. Matsukura, S. E. Barnes, S. Maekawa, and H. Ohno, Science **317**, 1726 (2007).
[2] S.-B. Choe and S.-C. Shin, Phys. Rev. Lett. **86**, 532 (2001).
[3] J. Pommier, P. Meyer, G. Penissard, and J. Ferre, P. Bruno, and D. Renard, Phys. Rev. Lett. **65**, 2054 (1990).
[4] W. Wernsdorfer, E. B. Orozco, K. Hasselbach, A. Benoit, B. Barbara, N. Demoncy, A. Loiseau, H. Pascard, and D. Mailly, Phys. Rev. Lett. **78**, 1791 (1997).
[5] H. W. Xi, K.-Z. Gao, J. O. Yang, Y. M. Shi, and Y. Z. Yang, J. Phys.: Condens. Matter **20**, 295220 (2008).
[6] S. M. Wu, W. Zhang, A. KC, P. Borisov, J. E. Pearson, J. S. Jiang, D. Lederman, A. Hoffmann, and A. Bhattacharya, Phys. Rev. Lett. **116**, 097204 (2016).
[7] H. Wang, C. Du, P. C. Hammel, and F. Yang, Phys. Rev. Lett. **113**, 097202 (2014).
[8] W. W. Lin, K. Chen, S. F. Zhang, and C. L. Chien, Phys. Rev. Lett. **116**, 186601 (2016).
[9] L. Frangou, S. Oyarzún, S. Auffret, L. Vila, S. Gambarelli, and V. Baltz, Phys. Rev. Lett. **116**, 077203 (2016).
[10] Z. Qiu, J. Li, D. Hou, E. Arenholz, A. T. N'Diaye, A. Tan, K.-i. Uchida, K. Sato, S. Okamoto, Y. Tserkovnyak, Z. Q. Qiu, and E. Saitoh, Nat. Commun. **7**, 12670 (2016).
[11] Q. Li, M. Yang, C. Klewe, P. Shafer, A. T. N'Diaye, D. Hou, T. Y. Wang, N. Gao, E. Saitoh, C. Hwang, R. J. Hicken, J. Li, E. Arenholz, and Z. Q. Qiu, Nat. Commun. **10**, 5265 (2019).
[12] P. Wadley, B. Howells, J. Zelezny, C. Andrews, V. Hills, R. P. Campion, V. Novak, K. Olejnik, F. Maccherozzi, S. S. Dhesi, S. Y. Martin, T. Wagner, J. Wunderlich, F. Freimuth, Y. Mokrousov, J. Kunes, J. S. Chauhan, M. J. Grzybowski, A. W. Rushforth, K. W. Edmonds, B. L. Gallagher, and T. Jungwirth, Science **351**, 587 (2016).
[13] P. Wadley, S. Reimers, M. J. Grzybowski, C. Andrews, M. Wang, J. S. Chauhan, B. L. Gallagher, R. P. Campion, K. W. Edmonds, S. S. Dhesi, F. Maccherozzi, V. Novak, J. Wunderlich, and T. Jungwirth, Nat. Nanotechnol. **13**, 362 (2018).
[14] S. Y. Bodnar, L. Smejkal, I. Turek, T. Jungwirth, O. Gomonay, J. Sinova, A. A. Sapozhnik, H. J. Elmers, M. Klaui, and M. Jourdan, Nat. Commun. **9**, 348 (2018).
[15] T. Moriyama, K. Oda, T. Ohkochi, M. Kimata, and T. Ono, Sci. Rep. **8**, 14167 (2018).
[16] X. Z. Chen, R. Zarzuela, J. Zhang, C. Song, X. F. Zhou, G. Y. Shi, F. Li, H. A. Zhou, W. J. Jiang, F. Pan, and Y. Tserkovnyak, Phys. Rev. Lett. **120**, 207204 (2018).
[17] L. Baldrati, O. Gomonay, A. Ross, M. Filianina, R. Lebrun, R. Ramos, C. Leveille, F. Fuhrmann, T. R. Forrest, F. Maccherozzi, S. Valencia, F. Kronast, E. Saitoh, J. Sinova, and M. Kläui, Phys. Rev. Lett. **123**, 177201 (2019).
[18] T. Jungwirth, X. Marti, P. Wadley, and J. Wunderlich, Nat. Nanotechnol. **11**, 231 (2016).
[19] H. W. Xi, S. Franzen, S. N. Mao, and R. M. White, Phys. Rev. B **75**, 014434 (2007).
[20] J. Dho, C. W. Leung, and M. G. Blamire, J. Appl. Phys. **99**, 033910 (2006).
[21] P. A. A. van der Heijden, T. F. M. M. Maas, W. J. M. de Jonge, J. C. S. Kools, and F. Roozeboom, Appl. Phys. Lett. **72**, 492 (1998).
[22] S. Polisetty, S. Sahoo, and C. Binek, Phys. Rev. B **76**, 184423 (2007).
[23] J. Wu, D. Carlton, J. S. Park, Y. Meng, E. Arenholz, A. Doran, A. T. Young, A. Scholl, C. Hwang, H. W. Zhao, J. Bokor, and Z. Q. Qiu, Nat. Phys. **7**, 303 (2011).
[24] R. Abrudan, J. Miguel, M. Bernien, C. Tieg, M. Piantek, J. Kirschner, and W. Kuch, Phys. Rev. B **77**, 014411 (2008).
[25] N. C. Koon, Phys. Rev. Lett. **78**, 4865 (1997).
[26] T. C. Schulthess and W. H. Butler, Phys. Rev. Lett. **81**, 4516 (1998).

[27] J. Wu, J. S. Park, W. Kim, E. Arenholz, M. Liberati, A. Scholl, Y. Z. Wu, C. Hwang, and Z. Q. Qiu, Phys. Rev. Lett. **104**, 217204 (2010).
[28] Q. Li, G. Chen, T. P. Ma, J. Zhu, A. T. N'Diaye, L. Sun, T. Gu, Y. Huo, J. H. Liang, R. W. Li, C. Won, H. F. Ding, Z. Q. Qiu, and Y. Z. Wu, Phys. Rev. B **91**, 134428 (2015).
[29] Q. Li, T. P. Ma, M. Yang, L. Sun, S. Y. Huang, R. W. Li, C. Won, Z. Q. Qiu, and Y. Z. Wu, Phys. Rev. B **96**, 024420 (2017).
[30] J. Zhu, Q. Li, J. X. Li, Z. Ding, C. Y. Won, and Y. Z. Wu, J. App. Phys. **114**, 173912 (2013).
[31] W. N. Cao, J. Li, G. Chen, J. Zhu, C. R. Hu, and Y. Z. Wu, Appl. Phys. Lett. **98**, 262506 (2011).
[32] I. V. Soldatov and R. Schäfer, Rev. Sci. Instrum. **88**, 073701 (2017).
[33] A. N. Kolmogorov and Izv. Akad. Nauk SSSR, Ser. Mat. **3**, 355 (1937).
[34] M. Avrami, J. Chem. Phys. **8**, 212 (1940).
[35] G. van der Laan, E. Arenholz, R. V. Chopdekar, and Y. Suzuki, Phys. Rev. B **77**, 064407 (2008).
[36] C. T. Chen, Y. U. Idzerda, H.-J. Lin, N. V. Smith, G. Meigs, E. Chaban, G. H. Ho, E. Pellegrin, and F. Sette, Phys. Rev. Lett. **75**, 152 (1995).
[37] R. Nakajima, J. Stöhr, and Y. U. Idzerda, Phys. Rev. B **59**, 6421 (1999).
[38] S. R. Ali, M. R. Ghadimi, M. Fecioru-Morariu, B. Beschoten, and G. Güntherodt, Phys. Rev. B **85**, 012404 (2012).
[39] J. Xu, C. Zhou, M. Jia, D. Shi, C. Liu, H. Chen, G. Chen, G. Zhang, Y. Liang, J. Li, W. Zhang, and Y. Wu, Phys. Rev. B **100**, 134413 (2019).